PCCP

Polaron-formation revealed by transient XUV imaginary refractive index changes in different iron compounds

Journal:	*Physical Chemistry Chemical Physics*
Manuscript ID	CP-COM-01-2021-000103.R1
Article Type:	Communication
Date Submitted by the Author:	03-Feb-2021

Complete List of Authors:	Chen, Wenfan; University of California San Diego, Material Science and Engineering Program Xiong, Wei; University of California, San Diego, Department of Chemistry and Biochemistry; University of California, San Diego, Materials Science and Engineering Program

COMMUNICATION

Polaron-formation revealed by transient XUV imaginary refractive index changes in different iron compounds

Wenfan Chen,[a] Wei Xiong [a,b]

/0,om,jkkkkksReceived 00th January 20xx,
Accepted 00th January 20xx

DOI: 10.1039/x0xx00000x

We use transient extreme ultraviolet (XUV) reflection absorption spectroscopy to study polaron formation on hematite and akaganeite surfaces. We observed a reduction in the offset of the imaginary refractive index (κ_{offset}) that was attributed to the photoemission cross-section. The difference in the κ_{offset} reduction indicated that deeper-trapped polarons were formed in hematite than in akaganeite.

In semiconductors, electron-hole pairs are often trapped by distorting the surrounding lattice and creating a local minimum potential, forming so-called small polarons. Small polarons reduce charge mobility and increase the chances of charge recombination, which deteriorates the performance of photo- and electrocatalysts. Many efforts have studied the activation energy and formation dynamics of polarons in order to provide principles to manipulate polaron formation in semiconductors[1–3].

Hematite (α-Fe_2O_3) is an ideal candidate for photo-catalytical applications, because of its high abundance and its visible band-gap at ~2eV[4,5]. A recent study found that small polarons caused the low charge mobility in hematite[6]. Therefore, hematite has been studied intensely in small polarons research. Leone et al. discovered the XUV spectral signature of small polarons in hematite[1,2]. They further studied the dynamics of polarons' dependence on the excited energy and concluded that excitation energy influenced polaron hopping efficiency. Baker et al. studied the surface polaron dynamics of hematite using transient XUV reflectance absorption (RA) spectroscopy and found that surface polaron formation is slower than bulk polaron formation[7]. Thus, much knowledge has been gained in terms of the energetics and dynamics of polaron formation.

[a] Materials Science and Engineering Program, University of California, San Diego.
[b] Department of Chemistry and Biochemistry, University of California, San Diego.
† Footnotes relating to the title and/or authors should appear here.
Electronic Supplementary Information (ESI) available: [details of any supplementary information available should be included here]. See DOI: 10.1039/x0xx00000x

However, less attention has been paid on trap depth and the lattice change associated with small polarons by transient XUV spectroscopy. Because XUV only provides the relative energy difference between the traps and core levels, and the core level energy also changes due to screening effect, it makes XUV less sensitive to the energy level of polaron states. Nevertheless, knowledge of these physical processes could provide a new aspect on engineering the carrier mobility. In this work, we show that transient XUV reflection absorption (XUV-RA) spectroscopy can reveal insights into the relative depth of polaron traps and the corresponding lattice expansion. In addition to hematite, we measured the dynamics of β-FeOOH (akaganeite), another candidate for solar water splitting and photocatalytic applications,[8,9] and aimed to reveal the differences in polaron dynamics between these two materials (material characterization can be found in ESI section S2).

To examine polaron formations on both hematite and akaganeite surfaces, we utilized transient XUV-RA spectroscopy. As shown by Baker and co-workers, transient XUV-RA spectroscopy is sensitive to surface polaron formation[10]. A table-top XUV setup is illustrated in Figure 1. The probe pulse was created by high harmonic generation under quasi-phase matching conditions, where an 800 nm beam and a 400 nm beam were combined and focused by a f=50 cm lens into a 2 cm*150 μm glass fiber filled with neon gas[11]. The mixing of two fields breaks the field symmetry, generating both even and odd order harmonics[2,7]. The XUV beam was focused by a toroidal mirror onto the sample surface. The XUV beam reflected by the sample was then dispersed by a laminar-type diffraction grating and detected by the XUV charge-coupled device (CCD) detector. The pump beam was generated by frequency doubling of the 800-nm beam with a beta barium borate (BBO) crystal (60 μJ). The 400 nm beam was focused onto the sample in an area of ~1 mm^2. Two Al foils (0.2 μm thickness, Lebow) were added before and after the sample to remove residual driving and pump pulses. The transient spectra (Fig. 2) were calculated by $\Delta OD = -log(I_{pumpon}/I_{pumpoff})$; the I_{pumpon} and $I_{pumpoff}$ are the measured XUV spectra from

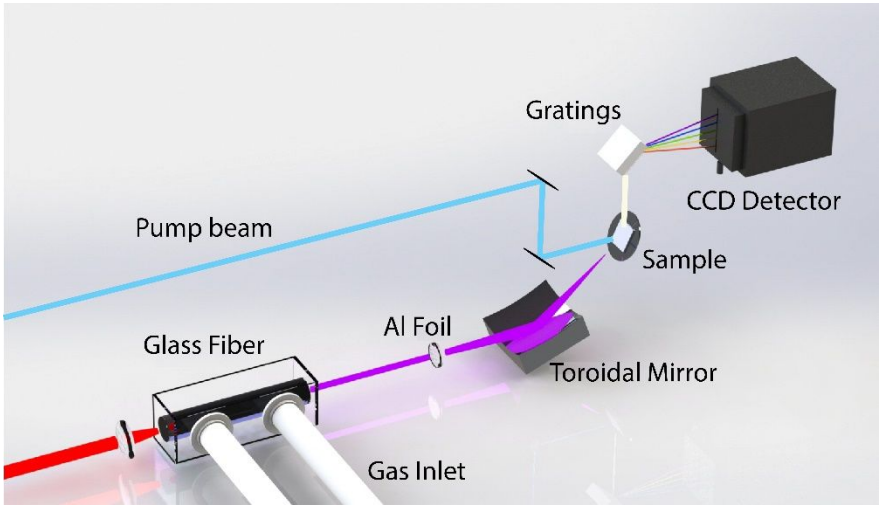

Figure 1. Table-top time resolved XUV RA spectroscopy setup. XUV was generated in the glass fiber driven by an 800 nm beam (1.2 mJ) and 400 nm beam (30 μJ). Neon was purged into the fiber; the pressure at the entrance is 200 mTorr. The residual driving beam was blocked by the Al foil. The XUV beam was focused onto the sample by a toroidal mirror (r_h = 14327 mm, r_v = 17.4 mm, ARW) and detected by CCD (DO940P-BEN, Andor) after being dispersed by the gratings (300 grooves/mm, Shimadzu). The sample is pumped by 60 μJ of 400 nm beam. The angle between the probe beam and the sample plane normal is 84°. The angle between the pump beam and the sample plane normal is 60°.

the reflection beam with pump laser incident on and off the samples.

To further quantify the dynamics of the two materials, we extracted spectral and dynamical components from the transient RA spectra by global analysis and multivariable regression. Global analysis was first performed to obtain the different spectral components using Glotaran[12]. Time traces of the initial state and final state were obtained by multivariate regression analysis of the raw transient spectra. The decomposed spectral features of the initial states of hematite and akaganeite (Fig. 3A and B) reflect the hot electrons in the conduction band after photo excitation. The final state corresponds to the polarons formed after hot electron relaxation[2]. Since the focus of this study is polaron formation, we explicitly analyse the final state spectra and dynamics.

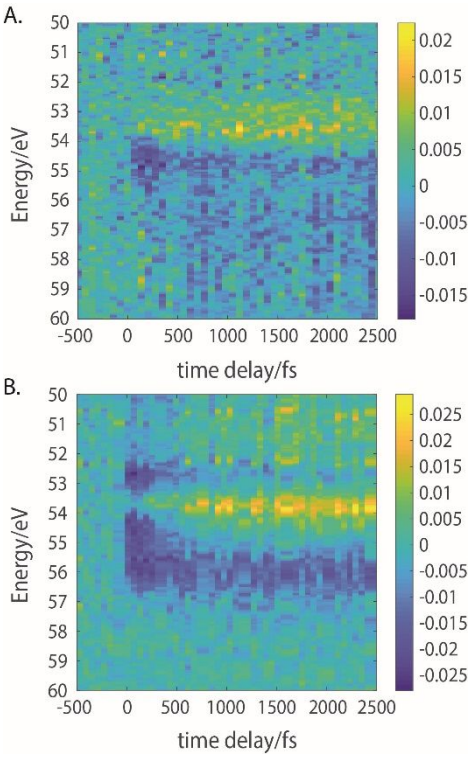

Figure 2. Contour plot of transient RA spectra of (A) hematite and (B) akaganeite. The z-axis of the color plot is ΔOD.

First, the polaronic spectral features are different between the two samples. Spectra for both materials, have a positive feature at about 54 eV. For hematite, there are two weak negative peaks at 55 eV and 57 eV separately, while for akaganeite, there is only one negative peak at 56 eV. Second, the two samples have different polaron formation dynamics. Using the two-temperature models[13], the fitted dynamics (detailed in ESI section S3) show the polaron formation time is 261 ± 65 fs and 429 ± 70 fs for hematite and akaganeite, respectively.

To reveal the origin of the final transient spectral difference, we simulated static and transient XUV RA spectra. We first used CTX4XAS[14] software to calculate the absorption coefficient of Fe3+. The imaginary part of the refractive index (κ) was then calculated from the absorption coefficient, and the real part (n) was derived from the Kramers-Kronig relation. The reflectance of hematite and akaganeite was then calculated by Fresnel equation (detailed procedure in ESI section S4). To simulate the static XUV reflectance of the two materials, we included non-resonant offsets to both n and κ for both materials and use the following equation $N(\omega)=n(\omega)+n_{offset}+i(\kappa(\omega)+\kappa_{offset})$ to calculate the complex refractive index N(ω). The n_{offset} and κ_{offset} applied on hematite was -0.15 and 0.32, respectively, and on akageneite was -0.15 and 0.20, respectively. The n_{offset} depends on the surface flatness[15], whereas the κ_{offset} is mainly contributed by the photoemission of the XUV pulses.

To further simulate the transient spectra, we calculated the difference between the ground and polaron states' RAs. The polaron state RA was calculated by replacing the refractive index of polarons into the Fresnel equation. The polaron-induced lattice expansion results in a splitting of core levels. We assume the splitting of the core levels are 0 eV and 2.5 eV with a weighting number of 2:1[16]. As electrons are localized at the Fe site, the charge transfer hybridization of Fe atoms is reduced

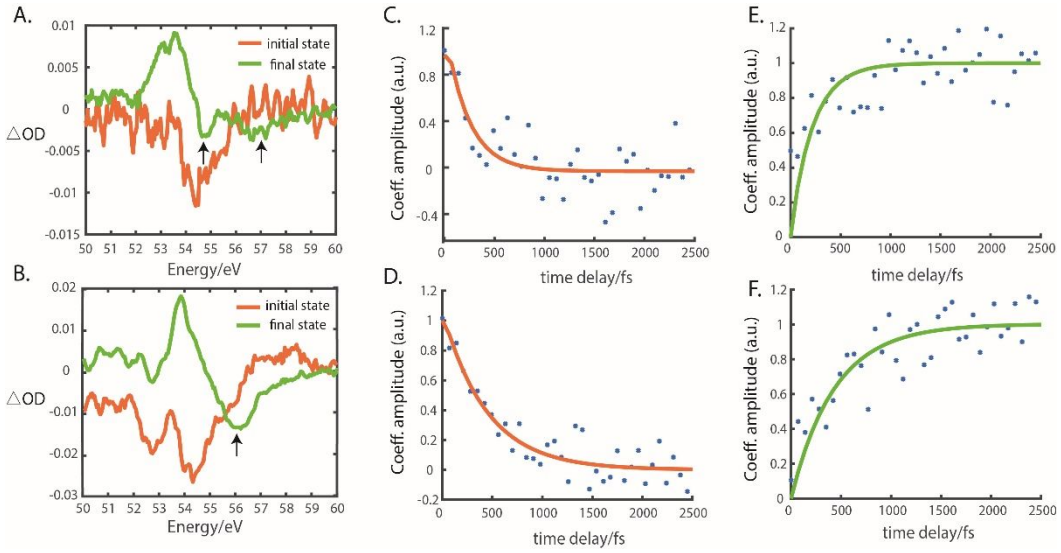

Figure 3. Initial and final state spectra of (A) hematite and (B) akaganeite extracted from global analysis. The arrows indicate the peak position. Time dynamics of initial states (C, D) and final states (E, F) were extracted using multivariable regression. The solid lines in (C-F) are fitting results using a two-temperature model.

compared to the initial excited state, i.e. the pure Fe^{2+} states only live for tens of femtosecond and the excited electrons become delocalized between oxygen and iron atoms[2]. Therefore, the conduction band density of the polaron state more closely resembles the ground state Fe^{3+} atom.[2,16] Thus, the polaron state refractive index was calculated by adding Fe3+ absorption coefficients of different core splitting and the non-resonance offsets together, which agrees with experimental data well. The exact electronic structure of the polaron subject further investigation by high level electronic structure calculations.

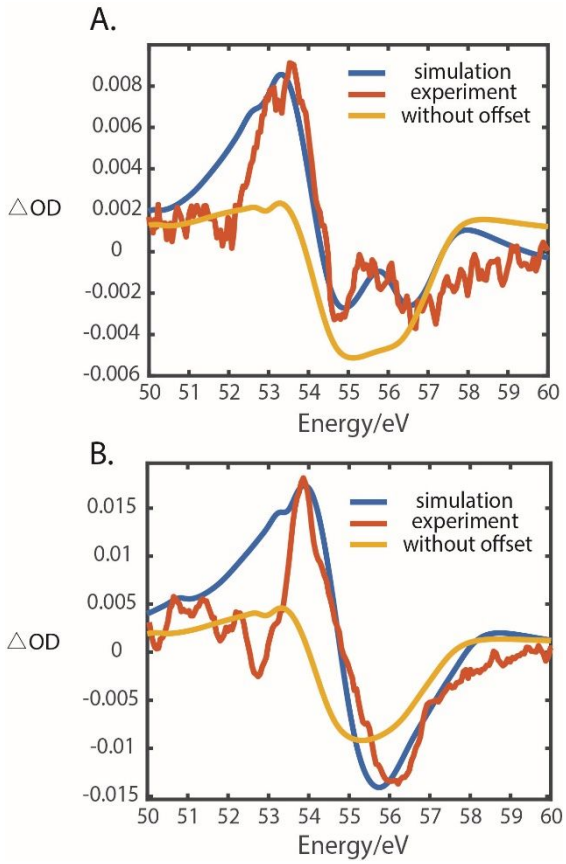

Figure 4. Simulated transient polaron state (final state) spectra of (A) hematite and (B) akaganeite. The refractive index offset change is critical to reproduce experimental results.

The non-resonant offsets become the key parameters to reproduce the transient spectral difference between hematite and akaganeite. To fit the double negative feature in the hematite spectrum (Fig. 4A), the κ_{offset} changes from 0.32 to 0.19. Correspondingly, to fit the single negative feature of akaganeite, the κ_{offset} reduces from 0.2 to 0.15 (Fig. 4B, see ESI Fig.S6 for offset dynamics). Clearly, without applying $\kappa_{offset,}$ the yellow trace in Figure 4 shows the simulation result cannot reproduce the experimental results. Meanwhile, the n_{offset} remains the same. Intuitively, when two peaks exists in the transient spectrum, it indicates that there is new state created. However, here, the two negative peaks could come from the offset change in the refractive index. We note that, to the best of our knowledge, this is the first time the effect of κ_{offset} changes are reported in transient XUV spectroscopy. The κ_{offset} changes were not reported in the transmission geometry of transient XUV, because, as discussed below, transient XUV in the RA geometry probes the surface, which is more sensitive to κ_{offset} that is related to surface photoemission.

While it is easy to understand why the n_{offset} did not change – within the time scale of this experiment, there cannot be any surface flatness changes – it is very interesting to observe significant changes in κ_{offset}. The κ_{offset} determines the off-resonant absorption coefficient, which is mainly due to photoemission. In previous two-photon photoemission experiments[17,18], researchers observed that when electrons in the conduction band thermalized into polaron states, the photoemission signals reduced dramatically. When polarons form, they lengthen the Fe-O bond length. The distorted lattice, in return, immobilizes the charges, because it undergoes significant lattice changes when the charges are removed either to the vacuum, which corresponds to photoemission, or to a neighbouring site that is related to charge mobility. Thus, the small photoemission cross-section of polarons can be explained by the localization and lattice distortion of polarons.

Since the κ_{offset} corresponds to non-resonant absorptions that lead to photoemission, the decrease of κ_{offset} indicates that charges in the polaron states are more trapped than those in the ground state, leading to a smaller photoemission cross section of polarons. This explanation of κ_{offset} change is consistent with the initial transient spectra shown in Fig. 3A and B, which are simulated with a slight increase of κ_{offset},(ESI section S5) reflecting hot electrons that are more easily photoemitted. Based on the above analysis, the larger κ_{offset} reduction (41%) of hematite compared to akaganeite (25%) implies that polarons are held deeper in hematite than in akaganeite. Correspondingly, polarons in hematite should introduce a larger lattice distortion.

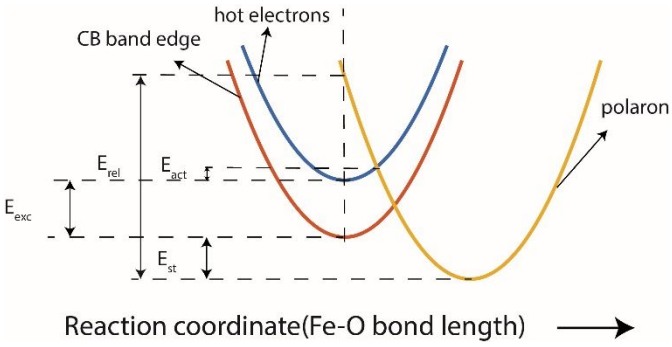

Figure 5. Marcus model for electron transfer during the polaron formation process. E_{act} is the activation energy, E_{st} is the self-trapping energy, E_{rel} is the relaxation energy, E_{exc} is the excess energy equals E_{pump}-E_{gap}

Having interpreted the transient XUV RA spectra, we now discuss the different polaron formation dynamics of these two samples. Polaron formation can be calculated using equation $k_{st} = \omega * \exp(-\Delta E_{act}/kT)$[19]. The relation between the polaron formation time of the two samples follows the equation $\tau_h/\tau_a = \omega_a/\omega_h * \exp(-(\Delta E_a - \Delta E_h)/kT)$, where ω_h and ω_a are the LO phonon frequency of hematite and akaganeite, the frequency for hematite and akaganeite are 50 fs[20] and 54 fs[21], respectively. ΔE_h and ΔE_a are the activation barrier energy of hematite and akaganeite. T is the lattice temperature at 600K, which has been previously estimated at similar excitation power density[1,3]. Then, the activation energy difference is $\Delta E_h - \Delta E_a = -25meV$, which agrees with previous theoretical predictions of mobilities[19,22].

Based on the Marcus theory (Fig. 5), the relaxation energy, E_{rel} can be determined from the activation energy by $\Delta E_{act} = (-E_{exc} - E_{st} + E_{rel})^2/4E_{rel}$,[23] where E_{st} is the self-trapping energy of polarons, and the excess energy E_{exc} equals the difference between the pump energy and the band gap. The band gap of hematite and akaganeite are 2.1 eV and 2.5 eV respectively, obtained from the UV-Vis spectra (ESI figure S3). The self-trapping energy of hematite is 0.32 eV[3,24]. Since there is a lack of knowledge of the self-trapping energy of akaganeite, we estimated that it should be less than that of hematite, based on the smaller change of κ_{offset} seen in akaganeite. We found that under this condition, the relaxation energy of hematite is always larger than that of akaganeite (ESI Sec. S6). This result implies that hematite undergoes a larger lattice expansion than akageneite, agreeing with the results from polaron transient spectra.

We note that the faster polaron formation rate seen in deeper trapped hematite is a net result of multiple energy variables in the Marcus model: hematite has both larger E_{st} and E_{exc}, which lead to smaller ΔE_{act}. It appears that reduction of ΔE_{act} due to these two factors is large enough to compensate for the ΔE_{act} increase due to a large E_{rel}, so that the ΔE_{act} in hematite is smaller than that in akaganeite.

In summary, we showed that the featureless refractive offset can change in transient XUV RA spectroscopy, which provides important insights into polaron trapping and lattice expansion, as well as additional knowledge regarding the electronic structure dynamics extracted from spectral lineshapes. This finding makes transient XUV RA spectroscopy further complement other techniques applied in polaronic research. For example, time-resolved THz spectroscopy can quantify the charge density and associated phonon modes during phonon formation dynamics[25]. Here we further show that transient XUV RA, aside from being element specific, is also sensitive to trapping depth and lattice expansion, which is not directly available in the aforementioned technique. The experimental results suggest that a deeper polaron state is formed in hematite than in akaganeite. Tracking this non-resonant offset change in transient XUV RA spectroscopy can be applied to study trap states in other metal complexes for optoelectronic, such as ITO and In_2O_3[26] and photocatalytic applications, such as Bi_2MoO_6 for water photoelectrolysis[27].

Conflicts of interest

There are no conflicts to declare.

Notes and references

Acknowledgement. This work is supported by AFOSR FA9550-17-1-0094. W.X. thanks L.R. Baker for the useful discussion of transient XUV RA setup, C. Chen for his help on the experiment, and G. Wiesehan for production of Figure 1. We thank J. Wang and Z. Yang for preparing the samples. Fabrication of the dual-cavity mirrors was done in part at the San Diego Nanotechnology Infrastructure of UCSD, a National Nanotechnology Coordinated Infrastructure site supported by the National Science Foundation (Grant ECCS-1542148).

1 I. J. Porter, S. K. Cushing, L. M. Carneiro, A. Lee, J. C. Ondry, J. C. Dahl, H. T. Chang, A. P. Alivisatos and S. R. Leone, *J. Phys. Chem. Lett.*, 2018, **9**, 4120–4124.

2 L. M. Carneiro, S. K. Cushing, C. Liu, Y. Su, P. Yang, A. P. Alivisatos and S. R. Leone, *Nat. Mater.*, 2017, **16**, 819–825.

3 S. Biswas, S. Wallentine, S. Bandaranayake and L. R. Baker, *J. Chem. Phys.*, 2019, **151**, 104701.

4 Y. Zhang, H. Zhang, H. Ji, W. Ma, C. Chen and J. Zhao, *J. Am. Chem. Soc.*, 2016, **138**, 2705–2711.

5 Y. Lin, G. Yuan, S. Sheehan, S. Zhou and D. Wang, *Energy Environ. Sci.*, 2011, 4, 4862–4869.

6 A. J. E. Rettie, W. D. Chemelewski, D. Emin and C. B. Mullins, *J. Phys. Chem. Lett.*, 2016, 7, 471–479.

7 J. Husek, A. Cirri, S. Biswas and L. Robert Baker, *Chem. Sci.*, 2017, **8**, 8170–8178.

8 Y. Zhao, H. Jiangyong and H. Chen, *J. Photochem. Photobiol. A Chem.*, 2010, **212**, 94–100.
9 C. Zhang, H.-C. Yang, L.-S. Wan, H.-Q. Liang, H. Li and Z.-K. Xu, , DOI:10.1021/acsami.5b02530.
10 A. Cirri, J. Husek, S. Biswas and L. R. Baker, *J. Phys. Chem. C*, 2017, **121**, 15861–15869.
11 C. Ding, W. Xiong, T. Fan, D. D. Hickstein, T. Popmintchev, X. Zhang, M. Walls, M. M. Murnane and H. C. Kapteyn, *Opt. Express*, 2014, **22**, 6194.
12 J. J. Snellenburg, S. Laptenok, R. Seger, K. M. Mullen and I. H. M. van Stokkum, *J. Stat. Softw.*, 2012, **49**, 1–22.
13 H. M. Van Driel, *Phys. Rev. B*, 1987, **35**, 8166–8176.
14 E. Stavitski and F. M. F. de Groot, *Micron*, 2010, **41**, 687–694.
15 A. Vincent, S. Babu, E. Brinley, A. Karakoti, S. Deshpande and S. Seal, *J. Phys. Chem. C*, 2007, **111**, 8291–8298.
16 Z. Wang and K. H. Bevan, *Phys. Rev. B*, 2016, **93**, 1–10.
17 T. J. S. Evans, K. Miyata, P. P. Joshi, S. Maehrlein, F. Liu and X. Y. Zhu, *J. Phys. Chem. C*, 2018, **122**, 13724–13730.
18 E. Varene, L. Bogner, C. Bronner and P. Tegeder, *Phys. Rev. Lett.*, 2012, **109**, 207601.
19 V. Alexandrov and K. M. Rosso, *J. Chem. Phys.*, 2014, **140**, 234701.
20 A. M. Jubb and H. C. Allen, *ACS Appl. Mater. Interfaces*, 2010, **2**, 2804–2812.
21 P. Colomban, S. Cherifi and G. Despert, *J. Raman Spectrosc.*, 2008, **39**, 881–886.
22 F. J. Morin, *Phys. Rev.*, 1954, **93**, 1195–1199.
23 N. H. Ge, C. M. Wong and C. B. Harris, *Acc. Chem. Res.*, 2000, **33**, 111–118.
24 S. Kerisit and K. M. Rosso, *Geochim. Cosmochim. Acta*, 2006, **70**, 1888–1903.
25 E. Cinquanta, D. Meggiolaro, S. G. Motti, M. Gandini, M. J. P. Alcocer, Q. A. Akkerman, C. Vozzi, L. Manna, F. De Angelis, A. Petrozza and S. Stagira, *Phys. Rev. Lett.*, 2019, **122**, 166601.
26 X. Yu, T. J. Marks and A. Facchetti, *Nat. Mater.*, 2016, **15**, 383–396.
27 J. Lyu, X. Liu, Y. Chen, H. Li, R. Li, X. Dong, H. Lee and H. Ma, *J. Phys. Chem. C*, 2020, **124**, 11525–11535.